# Photosensitive and Rare-Earth Doped Ceramics for Optical Sensing: A Review

B.G. POTTER JR. & M.B. SINCLAIR

*Sandia National Laboratories, Albuquerque, NM 87185-1405*

**Abstract.** This work reviews two inorganic materials classes used for optical sensors: photosensitive glasses and rare-earth doped materials. The underlying physical mechanisms contributing to the photosensitive response of germanosilicate glasses are discussed, along with a summary of optical sensor strategies which have been developed based upon photo-imprinted Bragg gratings. Particular attention is paid to the fabrication and characterization of photosensitive germanosilicate thin-films. Insights into the ability to control the photosensitivity of these materials through manipulation of material compositions and structures are also included. The discussion of rare-earth doped optical sensor materials emphasizes the important contribution of the host material to the observed optical behavior of the rare-earth ions. The use of rare-earth doped materials in applications ranging from temperature sensing to fiber-optic gyroscopes is also described.

Keywords: photo sensitivity, rare-earth, ceramics, optical sensors

## 1. Introduction

Sensing strategies based on measurement and retrieval of information through optical means provide significant advantages, and challenges, compared to electronically based approaches. Sensor elements, whose optical behavior is dependent on their immediate physical environment (e.g. the presence of a chemical specie or a change in the local temperature or stress state), can offer extremely high sensitivity and selectivity. Coupled with optical interrogation of the active element, an optical sensor system can provide high bandwidth, low cross-talk, low power consumption, remote operation, and insensitivity to electrical interference in a physically robust form. The often stringent requirements for good passive optical behavior and continued operation under adverse mechanical and chemical conditions, however, can be very difficult to satisfy.

The materials used in optical sensors can serve as the optical transducer elements, or, alternatively can provide the optical behavior necessary to interrogate the sensing element (e.g. spectroscopic light sources).

In some cases, both functionalities can be provided by a common material. The present work will focus on two classes of inorganic optical materials that have been the topic of a great deal of research both as sensor materials and, more generally, in the optical data manipulation and transmission field: photosensitive inorganic glasses and rare-earth doped materials. Both materials classes exploit the presence of point defects in an inorganic atomic structure to provide active optical sensing capabilities. Manipulation of both the defect structures themselves as well as the host material can dramatically impact the performance of, and deployment options for, sensors based on these materials.

It is important to stress that the choice of subject matter for the present work does not imply that these are the only ceramic materials that have been developed for optical sensor materials. Indeed, other extremely important classes of ceramic optical materials, including nonlinear optical materials such as $KTiOPO_4$, $BaTiO_3$, $LiNbO_3$, transition metal doped ceramics such as Ti:Sapphire or $Cr:Al_2O_3$, superconducting ceramics, and magnetic field sensing

materials such as yttrium iron garnet (YIG), have been used in a wide variety of physical and chemical sensors. However, space limitations prevent inclusion of these interesting and important material systems.

## 2.  Photosensitive Glasses

A major area of interest in inorganic materials-based optical sensors is the development of photo-imprinted refractive index structures in optical fibers and planar waveguides. These structures are formed through a photosensitive response intrinsic to the material. In general, traditional, inorganic glass formers, e.g. silica, germania and phosphate-containing glasses, are utilized although photosensitivity in nonoxide glasses has also been pursued [1–4]. By far the most technologically important materials in this area are germanosilicate glasses; these materials form the basis for readily available telecommunications-grade optical fiber and are, hence, ubiquitous in the photosensitivity literature. In the present section, a brief description of photosensitivity will be provided followed by an overview of microscopic mechanisms currently proposed to explain the photosensitive response in germanosilicate glasses. Materials processing concerns of consequence for photosensitivity will also be introduced. These topics will motivate a discussion of the primary photosensitive device structure formed in these materials: the Bragg grating. The use of photosensitive Bragg gratings as physical state sensing elements will then be reviewed. While primary emphasis will be placed on the body of work in optical fibers, the implications of planar waveguide-based Bragg grating sensors will also be examined. Recent work in our laboratory to evaluate new sensor applications for these materials is included.

### 2.1.  Background

Photosensitivity can be characterized as a stable, refractive index perturbation produced by exposure of the material to optical radiation. In the case of germanosilicate glasses, index changes of up to $10^{-3}$ can be efficiently fabricated within a germanosilicate glass through exposure to ultraviolet light, typically in the 190 nm to 340 nm wavelength range. While the precise mechanism causing the photosensitive effect will vary with material composition

(dopant additions or substitutions, oxygen stoichiometry), processing history and writing conditions, the phenomenon has been linked to optical absorption associated with point defect centers present within the glass structure (see later discussion). The effect was first observed in the Ge-doped core of silica-based optical telecommunications fibers in 1978 [5]. In this case, the 488 nm beam from an Ar-ion laser was used to produce a reflective grating through a two-photon absorption process.

Since this discovery, research in photosensitivity of inorganic glasses (fibers, fiber preforms, and waveguides) has spanned a wide range of material compositions, materials synthesis and processing routes, and photo-writing conditions. In addition to germanosilicates, photosensitivity has been examined in fibers containing a variety of other dopants (including phosphorous, boron, tantalum, and the rare-earths [6–9]). Planar waveguides formed using a variety of synthesis approaches including PECVD [10,11], sol-gel [12,13], flame hydrolysis [14], and sputtering [15–17] have also been investigated. As a result of this diversity in previous investigations, agreement on the mechanisms causing photosensitivity has not yet been attained. In fiber research, the unavoidable coupling of materials process parameters and material composition dictated by the fiber synthesis process itself makes a controlled materials study of photosensitivity very difficult. This issue, and the wide variety of exposure conditions currently employed in the field (e.g. UV pulse energies ranging from tens of mJ/(cm$^2$-pulse) to > 1 J/(cm$^2$-pulse); 190 nm to visible wavelengths) further occludes a unified description of the mechanisms involved. In general, however, it is agreed that the UV-photosensitive response in germanosilicate glasses is linked to the presence of oxygen-deficient point defect centers associated with germanium in the glass structure. Moreover, the optical absorption bands associated with these structures have been used to explain the wavelength dependence of the photosensitive response [18].

### 2.2.  Photosensitivity Mechanisms

Several mechanisms have been proposed to explain photosensitivity in germanosilicates. A color center model proposes that photoinduced refractive index changes are due to photo-induced charge transfer and trapping between defect complexes in the glass

(oxygen-deficient germanium centers). This process alters the optical absorption bands associated with the defects, which can be related to the refractive index changes via the Kramers-Kronig relations. It is important to note that modification of the optical absorption spectrum over a narrow spectral range can perturb the refractive index over the entire ultra-violet—near infrared spectrum. The primary absorption center has been assigned as an oxygen-deficient Ge-(Ge,Si) bond which absorbs at approximately 242 nm. This model has been used to successfully explain refractive index changes in some cases [19–21].

In addition to the color center model, mechanisms involving more dramatic optical modification of the glass structure have also been proposed. While the initial optical absorption is still believed to be associated with oxygen-deficient structural defects in the material, these models also include local heating and higher order absorption processes, which can cause modifications of the inherent stress state of the material [22] and even its density (compaction) [23]. The density change, for instance, is then the primary contributor to a refractive index. These effects have been substantiated through corroborative tests which showed changes in the dimensions of the material in areas subjected to UV-exposure [24] and TEM analyses which were interpreted as material densification resulting from strain relaxation [25]. These mechanisms are typically observed in materials exposed under high incident intensities ($> 50\,mJ/(cm^2$-pulse)) and/or high energy photons (e.g. $\lambda = 193$ nm) in an effort to increase the refractive index change produced. In addition to these more intrinsic materials phenomena are behaviors apparently linked to the fiber structure itself. Here, a grating structure can be imprinted at higher UV-pulse intensities ($> 30\,mJ/(cm^2$-pulse)) via damage produced at the core-clad interface [26].

From the findings available in the literature, it appears likely that all of the mechanisms proposed could contribute to the refractive index changes observed. The relative contributions, however, will depend on both the materials and the exposure conditions used. Based on the established link between the presence of oxygen-deficient defects and the photosensitive response, however, several post-synthesis methods have been utilized to increase the population of defect states associated with the bleachable absorption features through the introduc-

tion of hydrogen and a corresponding chemical reduction of the glass structure [13,27]. In the case of hydrogen loading (a high-pressure, moderate-temperature, hydrogen atmosphere treatment [27]), refractive index changes approaching $10^{-2}$ have been reported in the visible to near-infrared in optical fibers. This enhancement in photosensitivity is, however, temporary and can significantly degrade under ambient conditions (lower pressures) as the hydrogen incorporated into the glass structure diffuses out of the material.

## 2.3. Photosensitive Bragg Gratings

One of the most technologically important refractive index structures that can be imprinted into fibers or waveguides is the Bragg grating. These distributed feedback (DFB) gratings consist of a periodically varying refractive index pattern written along the waveguide core. Such gratings can provide extremely high reflectivities ($> 90\%$) over very narrow bandwidths. The peak reflectivity can be estimated, using coupled mode theory by the equation: $R = \tanh^2 (\pi\,\Delta n\,L/\lambda_o)$; where: $\Delta n =$ grating contrast, $L =$ grating length, $\lambda_o =$ wavelength at peak reflectivity, $R =$ grating reflectivity (normal incidence). Thus, even photoinduced refractive index modulations of less that $10^{-5}$ can provide high reflectivities if the grating length is sufficient. Depending on the writing conditions, gratings may extend along the entire length of a fiber or can be fabricated at specific locations. The reader is referred to past reviews which provide details concerning the various writing strategies that have been developed to fabricate Bragg gratings in fibers and waveguides [28,29]. Of primary importance is the development of a ''side-writing'' approach in which short length gratings are produced in the fiber core through the interference of two, coherent ultraviolet beams [30] (see Fig. 1).

Given the extremely narrow resonances typical of these structures, Bragg gratings provide highly selective reflectivity or transmission bandpass char-acteristics, making them very useful as wavelength selection devices and rejection filters. In addition, they can be used for dispersion compensation and as resonator cavity elements for in-fiber lasers. Indeed, the opportunity to provide highly integrable optical devices for optical telecommunications and optical signal manipulation systems is a significant driving force in the rapid evolution of the field. The area has,
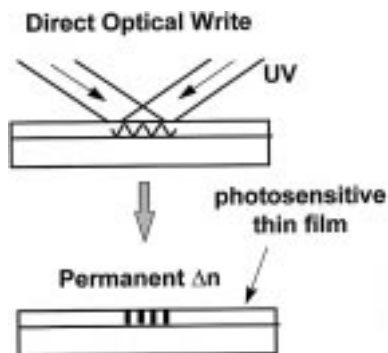
**Direct Optical Write**



*Fig. 1.* General side-writing geometry used to photo-imprint gratings into a photosensitive waveguide material. The angle between the two UV-beams will determine the periodicity of the interference pattern and, hence, the resulting Bragg wavelength for the index grating.

thus, commanded significant interest from the standpoint of the optimization of both fabrication routes and utilization strategies for specific applications [31,32].

### 2.4. Physical State Sensing

Photosensitive Bragg gratings written into optical fibers and waveguides can serve as very effective physical state sensors. Environmental influences, e.g. temperature and stress/strain fields, can modulate the optical response of the photosensitive grating structure through changes in the background refractive index and periodicity of the grating, thus providing a sensing element which can be interrogated optically. The utilization of photosensitive Bragg grating structures as sensors thus, is based on the interaction between the material in which the grating is written and on the local physical environment. Any disruption or modification of the periodicity or background refractive index will alter the reflection and transmission characteristics of the grating, e.g. the wavelength corresponding to the reflectivity peak of the grating. In the case of a strain field, an elongation or contraction of the grating will cause a shift in the peak reflectivity wavelength, or Bragg wavelength, $\lambda_b$, which, given the relatively narrow bandwidth of the grating, will produce a marked change in spectroscopic response. Thus, wavelength or frequency is a typically observed quantity for such sensing elements. Changes in local strain or temperature fields are transmitted to the

grating through the elastic, elastooptic and thermo-optic properties of the material itself. The sensitivity of the grating to such changes is therefore linked to these intrinsic properties as well as to the manner in which the material containing the grating is configured, i.e. physical constraints/arrangement geometry or intimate contact with another material. Photosensitive Bragg gratings have been examined for use as strain, vibration, temperature, and pressure sensors and accelerometers [33–38]. Typical values for sensitivity (defined as $\delta\lambda_b/\lambda_b$) to applied axial strain and temperature in optical fiber-based Bragg grating sensors are $7.64 \times 10^{-4}$/millistrain and $6.7 \times 10^{-6}$/C [31], respectively. In the case of fibers, the strain and/or temperature responses can be modified by jacketing or embedding the fibers in materials possessing alternate thermoelastic or mechanical properties. The approach can therefore be used either to enhance the sensitivity of the sensor or negate extraneous effects (e.g. temperature gradients) on the grating response. A similar approach could also be used for planar waveguide based sensors by depositing the photosensitive glass on substrates possessing desired properties.

Given the relative maturity of the grating writing process and the ability to fabricate gratings with specified Bragg wavelengths, grating arrays can be readily produced within a single optical fiber, forming a distributed sensor device which can provide spatial information regarding the physical state of the sampled environment. In general, the gratings are interrogated in a wavelength multiplexed manner [39]. Figure 2 illustrates this distributed sensor array concept for the case of optical fibers. These sensor arrays may be easily embedded into materials or composite structures allowing in-situ, remote optical monitoring of physical condition [40]. Such distributed arrays are also of interest for tamper-resistant tags and seals and as a means to insure the integrity of optical data transmission lines. In the latter case, the Bragg gratings could be written at wavelengths removed from the primary data transmission wavelength, allowing real-time interrogation of optical datalinks. A compromise in fiber integrity, indicated by splicing, breaking or movement (vibration) would be immediately evident in the spectral signature of the grating array. Moreover, a designed-in correspondence between the location of a grating and its Bragg wavelength, could provide the location of such a disturbance.
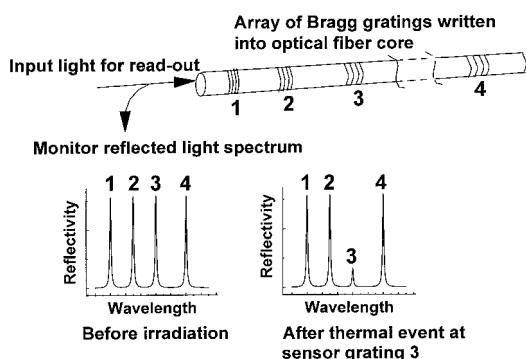
*Fig. 2.* Schematic depicting a distributed physical state sensor which employs an array of Bragg gratings imprinted within an optical fiber. In this case, the Bragg wavelength of a given grating element is correlated with its position along the fiber length thus providing position sensitive capabilities. Local environmental disturbances (e.g. thermal excursions) near a given grating element will modify its optical signature as observed during read-out with a broad-band optical source. Other events, e.g. vibration, would also provide similar feedback. The loss of portions of the fiber would be directly indicated by the absence of sections of the overall grating optical signature corresponding to those gratings lost from the fiber.

## 2.5. Planar Waveguide-based Photosensitivity

While planar waveguide-based, Bragg grating sensors have not been pursued as aggressively as fiber-based sensors, their potential is similarly high. Such elements could be integrated into small-scale, high areal density optoelectronic or integrated optical circuitry. The resulting systems could form the basis for extremely small, physically robust sensors which could be employed for a wide range of applications. Alternatively, such elements located ''on-chip'' could be used for self-evaluation of the physical state of the circuitry itself for lifetime estimation under adverse or rapidly changing conditions or even during circuit fabrication. Such integration, however, will ultimately depend on both materials and process compatibility between the photosensitive glass and the other materials which comprise the integrated device structure. In fact, efforts to incorporate such structures in photonic integrated circuitry for telecommunications functions are currently addressing these types of issues [10,41].

Thin film photosensitive germanosilicate glasses have been fabricated using a number of methods, including sol-gel [12,13], flame hydrolysis [42], PECVD [10,11], and sputtering from both oxide [15] and metallic alloy [16,17,43,44] targets. Given the established link between material atomic structure and photosensitivity, the variety of thin film deposition methods available for the formation of these glasses affords a unique opportunity to optimize the photosensitive response and the passive optical behavior of the resulting waveguide devices. An enhancement in photosensitivity can greatly impact the utility of these materials, providing higher density integrated devices or even enabling new functional modes, e.g. out-of-plane diffractive elements. In fact, significant photosensitivity ($\Delta n$ up to $10^{-3}$) has been realized in thin film germanosilicate materials both with [20] and without [10,16,17,43] post-synthesis hydrogen loading. Under low incident energy photo-writing condition, the UV-sensitive behavior of these materials has been consistent with that observed in optical fibers using the color-center mechanism interpretation [13]. Elevated pulse energies, however, can result in ablation of the material from the substrate [45].

Of particular note from the standpoint of materials providing low waveguide losses while still delivering reasonable photosensitivity are materials formed via plasma-enhanced chemical vapor deposition (PECVD). In this case, Bragg gratings have been written into Ge-doped waveguides patterned using reactive ion etching [10,41]. In addition to refractive index changes sufficient to provide high reflectivity DFB gratings ($\Delta n$ up to $2 \times 10^{-3}$ (at 1550 nm)), overcladding of such waveguides has provided waveguide losses down to 0.1 dB/cm [10]. An understanding of the origins for the high, as-deposited, photosensitivity exhibited in these materials has not been developed. Efforts have been primarily focused on optimization of the deposition conditions required to produced high-quality waveguides for technological applications.

Recent work within our laboratory has focused on an alternate deposition approach, reactive atmosphere RF-sputtering. This approach is driven by the known dependence of photosensitivity on the presence oxygen-deficient, germanium defect states. In this case, the germanosilicate glass is formed via sputtering from a Si/Ge alloy target under a partial oxygen atmosphere [16]. Variation in both the oxygen partial pressure during deposition and other deposition conditions (e.g. substrate temperature) have resulted in an ability to control both the population and characteristics of the defect states in the material

as evidenced by an integrated spectroscopic study [17]. The approach thus enables the photosensitivity of the glass to be tailored during synthesis without the need for post-synthesis processing and the inclusion of hydrogen into the structure. In fact, through substrate temperature variation, we have demonstrated an ability to produce either positive or negative refractive index changes in the visible and near infrared with a maximum refractive index change observed to date $= -4 \times 10^{-3}$ at 1.5 $\mu$m. This enhancement is attributed to marked changes in the UV-bleaching behavior exhibited in these films which results in corresponding variation in the UV-induced refractive index change as described by the Kramers-Kronig relations. We have successfully demonstrated both in-plane and out-of-plane diffraction as well as the ability to write large-core, embedded strip waveguides [43,44]. Losses are still being optimized, with the lowest losses measured to date of approximately 0.7 dB/cm at 632.8 nm.

This research has also indicated a novel sensor application for photosensitive Bragg gratings in general: ionizing radiation sensing. The new strategy is based on the inherent propensity for photoionization of defect states within the material which is responsible for the photosensitivity itself. We have observed significant changes in the UV-absorption characteristics of both virgin, RF-sputtered thin films and films previously UV-exposed (optically bleached) when subjected to a radiation dosage of at least 200 krad using 2 MeV X-rays. In fact, the X-ray induced absorption change is dependent on the prior UV-exposure history of the material, i.e. we see an absorption recovery in the UV-exposed material and a bleaching in the virgin material. The corresponding refractive index changes calculated using the Kramers-Kronig approach indicate that a significant change in contrast would be observed in a photosensitive Bragg grating due to local variability in the materials response to X-ray irradiation. Initial calculations indicate that grating reflectivity could drop by as much as 65% in a 15 mm long Bragg grating in our materials [46]. Thus, the intrinsic ionizing radiation sensitivity of the material (e.g. the absorption response) is amplified through the use of the Bragg grating structure. This general behavior is also expected in germanosilicate materials produced using other synthetic routes. However, the response is most likely enhanced in materials in which color-center-based refractive index modulations occur.

## 2.6. Summary

Photosensitivity in inorganic glasses has proven to be an extremely powerful approach for the integration of photonic device structures into both fibers and waveguides. The approach allows microphotonic devices to be patterned into an existing material ''blank'' using a single, direct optical writing process which, in general, does not require multistep chemical or mechanical processing. While a large body of work has been driven by telecommunications and optical signal processing applications, the coupling of small changes in the local physical environment to the optical response of photosensitive Bragg gratings (through the intrinsic mechanical, thermal and optical material properties) has enabled the design and synthesis of extremely sensitive physical state sensors. Although a majority of effort in the sensing area involves fiber-based structures, photosensitive glass thin films can provide additional opportunities for the application of Bragg grating-based sensor elements in high areal density applications such as photonic integrated circuits.

Thin film deposition approaches, moreover, can allow greater flexibility in material composition and processing, enabling enhanced photosensitivity leading to new functional modes and applications, beyond those based on distributed feedback gratings. Such technological strides, however, depend upon the elucidation of the photosensitive mechanisms themselves through well-controlled materials and processing studies. Increased understanding of the intrinsic mechanisms responsible for photosensitivity will not only contribute to enhanced performance but also to the ability to predict material and device structure lifetimes and viability under a variety of deployment conditions.

## 3.  Rare-Earth Doped Materials

### 3.1.  Background

Rare-earth doped materials are used in a large number of optical devices including light sources, lasers, phosphors and optical sensors. The widespread use of rare-earth materials is due in part to the large number of absorption and emission bands available using the various rare-earth elements, and also to the ease with which rare-earth dopants can be incorporated into a

large number of high quality crystalline and amorphous hosts. In this section, we will focus on the two most common uses of rare-earth doped materials in optical sensors: temperature sensing and light sources. We will begin by briefly reviewing several important aspects of the optical properties of rare-earth doped materials to provide background information for subsequent discussions. Then, we will consider temperature sensors which capitalize on the temperature dependence of the absorption and emission characteristics of certain rare-earth doped phosphors and glasses. Finally, we will discuss the use of rare-earth light sources in sensor applications.

### 3.2. Optical Properties of Rare-earth Doped Materials

Rare-earth dopants are typically incorporated into optical materials as trivalent ions [47], for which the number of 4f electrons increases from 1 for $Ce^{3+}$ to 13 for $Yb^{3+}$. Most of the interesting and useful optical properties of rare-earth doped materials are due to optical transitions between the 4f electronic levels of the rare-earth ions. The energies at which these transitions occur are only weakly affected by the host material, since the 4f electrons are effectively screened by outer, filled electron shells [48]. Thus, these transitions will appear at approximately the same wavelengths for a wide variety of host materials. The screening of the 4f electrons also reduces broadening of the f-f transitions due to environmental effects, and as a result, the absorption and emission spectra of rare-earth doped materials are characterized by narrow-line transitions. However, these spectra can be quite complex, since up to 13 electrons of the unfilled 4f level can participate in the optical transitions. A simple energy level diagram for several rare-earth ions is shown in Fig. 3.

Although the energies and line-widths of the f-f transitions are relatively insensitive to the local environment of the rare-earth ion, two important aspects of the optical behavior of the ions are determined by the host material. Electric dipole transitions between 4f states are strictly forbidden for an isolated ion, since the parity of the electronic configuration must change with an electric dipole transition. When the ion is incorporated into a host material, the presence of the local "crystal field" causes mixing of the 4f levels with states of different parity which enables electronic dipole transitions
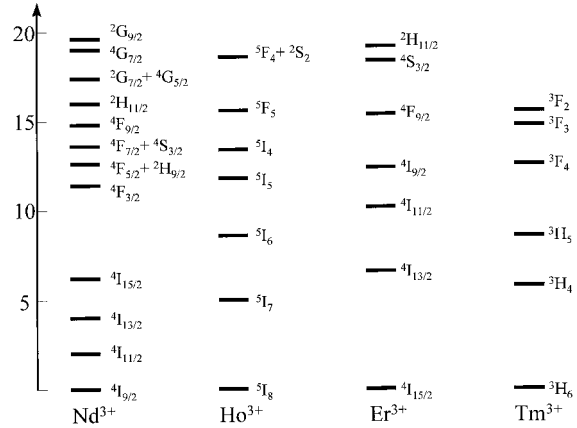


Fig. 3. A simple energy level diagram, adapted from [48] for $Nd^{3+}$, $Ho^{3+}$, $Er^{3+}$, and $Tm^{3+}$ ions.

between the levels [48]. However, the strengths of these electric dipole transitions remains relatively weak due to the perturbative nature of the state admixing, and, as a consequence, the radiative lifetimes of excited rare-earth ions can be relatively long ($\sim 10^{-3}$ s).

Another aspect of the behavior of the rare-earth ions that is determined by the host material is the rate of nonradiative relaxation of the excited states of the ions. The topic of nonradiative relaxation has been the subject of numerous theoretical and experimental investigations [49,50]. These works have shown that nonradiative relaxation proceeds via emission of multiple phonons. The probability of relaxation in this manner decreases exponentially with the number of phonons that must be emitted to span the energy gap between adjacent levels. If the energy gap is large relative to the characteristic phonon energy of the host, the probability of nonradiative relaxation is low since it requires the emission of a large number of phonons. Conversely, this process can proceed quite rapidly for closely spaced levels or high phonon energies. For certain ion/host combinations, the temperature dependence of multiphonon nonradiative relaxation can be quite pronounced, a feature which can be exploited in temperature sensing.

Once a rare-earth ion is promoted to an excited state, there are several possible processes that can occur during the relaxation to the ground state. First, direct radiative relaxation to a lower energy level of the 4f manifold can occur, with the emission of a

characteristic photon. Second, the ion can undergo multiphonon nonradiative relaxation to a lower level from which photon emission or further nonradiative relaxation can occur. In many important cases, such as the Nd:YAG laser, the rare-earth ion is photoexcited to a relatively high-lying state which relaxes via a cascade of multiphonon emission events to an intermediate level that is widely separated from the next lower level [49,51]. The intermediate level then relaxes via photon emission to a level near the ground state.

Another important process that can affect the relaxation of an excited ion is the transfer of excitation energy to a nearby ion via short-range multipole interactions between the ions. This process is known as energy transfer [48,52–54]. As the concentration of rare-earth ions increases, the average spacing between the ions decreases, and the importance of energy transfer increases. For sufficiently high concentrations, energy transfer can lead to a quenching of the quantum efficiency for photon emission by allowing the excitation energy to migrate to defect sites which cause rapid nonradiative de-excitation [55]. For many systems, this mechanism determines the upper limit of the dopant concentration.

However, energy transfer is not always detrimental to device performance, and in some cases this process can be manipulated to improve performance. For example, a host material might be deliberately doped with more than one rare-earth ion, with each ion chosen to perform a different function. One dopant might be chosen that has a strong absorption line that matches a convenient excitation source (such as a diode laser), while another dopant might be chosen to have an emission line at a desired wavelength. In this strategy, optical energy is absorbed from the excitation source by the first ion, transferred to the second ion, and the second ion emits at the desired wavelength. An example of such a system is a Tm,Ho co-doped silica fiber in which the $Tm^{3+}$ ions impart strong absorption in the 800 nm region and allow efficient photoexcitation using semiconductor diode lasers [56]. The energy of the $^3H_4$ [57] excited state of the $Tm^{3+}$ ion is very similar to the $^5I_7$ excited state of the $Ho^{3+}$ ion, and resonant energy transfer to the $Ho^{3+}$ ion is probable. In this manner, a significant fraction of the excitation energy supplied by the diode laser is transferred to the $Ho^{3+}$ ions, which emit efficiently near 2 μm. An energy level diagram depicting this process is shown in Fig. 4.
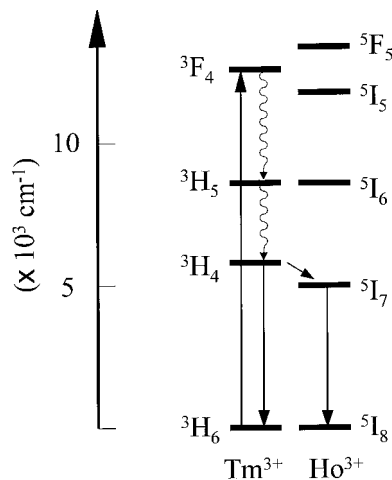


Fig. 4. An energy level diagram showing the photoexcitation of an $Ho^{3+}$ ions, followed by resonant energy transfer to $Tm^{3+}$ ion (after reference 56).

## 3.3. Temperature Sensors

One of the most widespread applications of rare-earth doped materials as sensors is in the field of temperature sensing [58]. Although there are a number of distinct ways that rare-earth doped materials can be used to sense temperature, they all make use of the influence of temperature on the absorption or emission characteristics of the rare-earth ions. This section will describe several different optical temperature sensors which utilize rare-earth doped materials. For each sensor system described, the materials used will be discussed along with a discussion of the thermal processes which are responsible for modifying the optical behavior.

Perhaps the most well-developed temperature sensors employing rare-earth doped materials are thermographic phosphors. The properties and uses of these phosphors have been extensively reviewed recently [59]. These phosphors are typically used in the form of powders of rare-earth doped crystallites such as $Eu:Y_2O_3$ and Tb:YAG [59]. They exploit the temperature dependence of the rate of nonradiative relaxation of the excited states of the rare-earth ions which, in general, increases as the temperature is increased. There are several physical mechanisms which can lead to an overall increase in the rate of nonradiative relaxation, such as the temperature dependence of the multiphonon nonradiative relaxa-

tion process described above [49,50]. Another mechanism which has been shown to lead to this type of behavior is thermal promotion to a higher lying charge transfer state that undergoes extremely rapid nonradiative relaxation [59]. Regardless of the mechanism, an increase in the nonradiative relaxation rate causes the overall relaxation rate to increase, since the nonradiative channel is in parallel with the radiative relaxation channel. The result is that both the emission lifetime and the quantum yield for radiative emission decrease with increasing temperature.

The temperature at which the nonradiative relaxation rate begins to compete significantly with the radiative relaxation channel depends upon the precise details of the energy levels of the rare-earth ion and the host environment. The range of temperatures for which the emission properties are most sensitive to temperature will vary for different ion/host combinations, or even for different excited state levels of the same ion. For example, the 611 nm emission line of the phosphor $Eu:Y_2O_3$ is a good choice for temperature sensing between $\sim 800$ K and $1400$ K [59], while the $Eu:La_2O_2S$ can be used at lower temperatures ($\sim 300$ K to $600$ K) [59]. Thus, through appropriate choice of phosphors, the thermographic phosphor technique can be used to measure temperature over a wide range of temperatures.

In a temperature sensing application, the thermographic phosphors are brought into thermal contact with the medium to be measured. This can be done by applying a coating of the phosphor powder to the surface of interest [59]. The phosphor coating can then be remotely interrogated using laser excitation. This approach has tremendous advantages since it enables temperature measurements of moving samples, as well as samples in harsh environments. Alternatively, the phosphor coating can be applied to the tip of an optical fiber which is brought into thermal contact with the sample [59]. In this approach, the interrogating beam is guided from the source to the phosphor, and the photons emitted by the rare-earth ions in the phosphor are guided by the fiber to the detection system.

For thermographic phosphors that capitalize on thermal quenching of the rare-earth luminescence, temperature can be determined by measuring the relative quantum efficiency for emission. However, in practice there are many factors which can degrade the accuracy of this type of measurement. A much simpler and more reliable method is to measure the relative linestrengths of two emission lines that exhibit different thermal behavior [59]. In this manner, a self-referenced determination of the emission linestrength is obtained which can be compared to previously recorded calibration data. Another attractive method to probe the phosphors is to measure the lifetime of the excited state of the rare-earth ions [59]. As mentioned above, the increase in the rate of nonradiative relaxation is manifested as a decrease in the emission lifetime of the rare-earth ions. A readout system based upon emission lifetime requires the use of a pulsed excitation source and time resolved detection electronics. Fortunately, the emission lifetimes are sufficiently long ($\mu$s–ms) that extremely high speed sources and electronics are not necessary.

Examples of the use of thermographic phosphors for temperature measurements include : measurement of the temperature of various components within jet engines, including moving components such as turbines; measurement of the temperature of the rotor surfaces within gas turbines; measurement of the rotor temperatures of electrical generators; and measurement of aerodynamic surfaces in wind tunnel tests [59].

A variety of strategies have been developed to utilize rare-earth doped optical fibers in temperature sensing applications. One approach has been to rely on temperature induced changes in the absorption characteristics of the rare-earth ions [60,61]. In one investigation [60], directed toward determining the feasibility of using rare-earth doped fibers to measure spatially averaged temperatures for building temperature control systems, optical fibers containing $Nd^{3+}$, $Pr^{3+}$, $Sm^{3+}$, and $Yb^{3+}$ were prepared using an MCVD process. The near infrared absorption spectra of these fibers were recorded as a function of temperature. The absorption spectra were found to evolve with temperature due to two mechanisms. The first mechanism is the change in the equilibrium population distribution of the rare-earth energy levels with temperature. At zero temperature, all rare-earth ions are in their ground states, and the absorption spectrum is characterized only by transitions that originate with the ground state. With increasing temperature, the width of the Boltzman distribution increases, and low-lying energy levels begin to become populated. In this case, the absorption spectrum will begin to exhibit absorption lines that originate on these low-lying states. As the temperature

increases further, the strength of these absorption lines grows. The second mechanism responsible for modifying the absorption spectrum is a slight shifting of the energy levels with temperature, due to thermally induced changes in the local environment experienced by the rare-earth ions. This mechanism leads to an increase in absorption on one side of the absorption line, and a corresponding decrease in absorption on the other side of the line.

For each rare-earth doped fiber used in [60], the thermally induced changes in the absorption spectrum were measured, and used to determine wavelength pairs which optimize the sensitivity of the sensors in differential measurements. This investigation concluded that spatially averaged temperature measurements with a resolution of $+/- 1°C$ in the range from 0 to 100°C is feasible with $Nd^{3+}$ and $Pr^{3+}$ doped fibers. In a similar investigation, it was shown that the temperature-dependent absorption characteristics of $Yb^{3+}$ doped silica core fibers can be used as the basis for a temperature sensor [61].

Distributed (i.e. spatially resolved) temperature measurements which exploit the temperature dependent absorption characteristics of rare-earth doped fibers are also possible. This can be achieved by launching a short laser pulse down one end of a rare-earth doped fiber, and monitoring the temporal dependence of the return signal due to Rayleigh backscattering using conventional optical time domain reflectometry (OTDR) techniques. The laser pulse is attenuated as it propagates down the fiber due to rare-earth absorption, and due to Rayleigh scattering. A fraction of the scattered photons are captured by the fiber and propagate back toward the excitation source. These ''return'' photons are also attenuated by rare-earth absorption as they propagate back to the source. The spatial distribution of the loss within the fiber can be calculated by measuring the temporal characteristics of the return signal from both ends of the fiber, and since the local loss of the fiber is dependent upon temperature, the spatial temperature profile can be calculated. The wavelength of the laser pulse must be chosen to be in the vicinity of a rare-earth absorption line, so that temperature dependent absorption can influence the propagation of the pulse. However, if the wavelength occurs in a region of strong rare-earth absorption, the laser pulse will be attenuated after a short length of fiber, and the sensor will not be capable of measurement over large distances. To satisfy these two requirements, the operating wavelength is typically placed on the tail of one of the rare-earth absorption lines.

An early demonstration [62] of spatially resolved temperature sensing employed a $Nd^{3+}$ doped fiber, optimized for a 200 m length. The operating wavelength was chosen to be 904 nm. A pulsed laser diode (40 ns) was used as the excitation source, and conventional OTDR instrumentation was used to monitor the return signal. A temperature accuracy of 2°C was obtained with a spatial resolution of 15 m over a range of 140 m, demonstrating the feasibility of this approach.

The optical emission from rare-earth ions has also been employed in fiber optic temperature sensors. In one investigation of this type [63,64], the luminescence intensity ratio of two rare-earth emission lines was measured as a function of temperature for an $Er^{3+}$ doped fiber. The emission lines used were the $^2H_{11/2}$–ground state ($\sim 530$ nm) and $^4S_{3/2}$–ground state ($\sim 550$ nm). The upper levels of these two emission lines are separated by a relatively small energy gap of $\sim 750$ cm$^{-1}$, which allows for fast thermalization between the two levels. At low temperatures, only the lower of these levels ($^4S_{3/2}$) will be populated, and the emission is expected to occur primarily from this level. As the temperature is increased, the population of the upper level ($^2H_{11/2}$) will increase, increasing the emission intensity from this level. Errors due to fluctuations in the excitation intensity are small, since the self-referenced ratio of the emission from these lines is measured. In an experimental demonstration of point temperature sensing using this mechanism, light from a Ti:Sapphire operating at 800 nm was used to generate luminescence from a 2 cm length of silica-core fiber doped with 2500 ppm of $Er^{3+}$. The counter-propagating luminescence intensity ratio was found to vary in a thermally activated manner. A total variation of 11 dB, was recorded over the temperature range from room temperature to 600°C, demonstrating the potential of this type of temperature sensor.

## 3.4. Light Sources for Sensor Applications

The wide variety of emission wavelengths available utilizing the various rare-earth ions, coupled with the ability to photo-pump the fibers using laser diodes, makes these solid-state light sources attractive for a number of optical sensing applications. The characteristics of the emission produced by rare-earth

doped optical fibers can vary widely, depending upon the dopant ions, the photoexcitation intensity, and the optical configuration. Fibers can be pumped below the gain threshold to produce temporally incoherent emission with limited brightness. More intense incoherent emission can be obtained by pumping the fibers just above the gain threshold, so that the rare-earth emission along the fiber direction is amplified by the process of amplified spontaneous emission. Light sources of this type are known as ''superluminescent light sources.'' If the fiber is pumped above the gain threshold and sufficient optical feed back is provided, lasing can occur. In this case intense, temporally coherent emission can be obtained from the fiber. In all cases, the emission from the fiber can possess a high degree of spatial coherence, since it is generated within the small core of the fiber and is spatially filtered to coincide with the fundamental mode of the fiber as it propagates (assuming single mode operation).

A straightforward application of rare-earth doped fibers to optical sensing takes advantage of the ability or rare-earth ions to generate bright emission in near infrared bands which overlap absorption bands of $H_2O$ and many organic compounds. For example, Tm-Ho co-doped silica fibers exhibit a luminescence band extending from 1.6 to 2.1 $\mu$m, which overlaps the absorption bands of compounds such as carbon dioxide, methane, arsine, and nitrous oxide [56]. As mentioned above, co-doping of the fiber with Tm and Ho enables optical pumping with semiconductor diode lasers operating near 800 nm due to absorption by the $Tm^{3+}$ ions. A fraction of the excitation energy of the $Tm^{3+}$ ions can be transferred to the $Ho^{3+}$ ions by the process of nonradiative energy transfer. Thus, the infrared emission from a co-doped fiber is quite broad, due to contributions from both rare-earth ions. In a sensing demonstration, the emission from a fiber of this type was used to measure the absorption of $CO_2$ molecules near 2 $\mu$m. Levels as low as 2% $CO_2$ were readily detected.

Another sensor demonstration which utilized the infrared emission of rare-earth ions employed a Tm-doped fluorozirconate fiber [65,66]. The low phonon energy characteristic of fluoride glasses drastically reduces the rate of multiphonon nonradiative relaxation of the rare-earth ions and thus greatly enhances the brightness of the infrared emission. Once again, diode laser pumping is possible due to the $^3H_6$ to $^3H_4$ [57] absorption line of $Tm^{3+}$. The emission spectrum

of this light source was shown to strongly overlap the absorption spectrum of liquid water. Two types of water sensors employing diode-pumped, Tm-doped optical fiber light sources were demonstrated. In the first demonstration, the infrared emission was coupled out of the fiber and directed through a variable path-length cell containing liquid water. The ratio of the infrared power to the residual pump power (at 780 nm) was measured after the water cell. With this configuration, path length differences as small as 1 $\mu$m were detectable. In the second sensing configuration, the emission from the Tm-doped fiber was coupled into a large core (600 $\mu$m) fiber from which the cladding had been removed. The large core fiber passed through a sample cell containing mixtures of water and methanol. In this configuration, absorption of the infrared light propagating along the fiber can occur due to the evanescent tails of the modes of the fiber. The effective absorbance of this optical configuration was found to vary linearly with the fraction of water in the mixture, demonstrating the potential of this type of sensor for sensitive concentration measurements.

The final application of rare-earth doped optical fibers that will be described here lies in the field of fiber optic rotation sensing and fiber optic gyroscopes [67], where superluminescent Er-doped fiber light sources have been successfully employed [68,69]. In a typical superluminescent light source for rotation sensing, the Er-doped fiber is photoexcited slightly above the gain threshold by a semiconductor diode laser. A fraction of the spontaneous emission from the $Er^{3+}$ ions is captured in the fundamental mode of the fiber, and is amplified as it propagates along the fiber. The intense, spatially coherent, but temporally incoherent, emission generated in this manner is then coupled into the rotation sensor. The primary advantage of using this type of light source is the low temporal coherence of the $Er^{3+}$ emission which drastically reduces readout noise associated with coherent Rayleigh backscattering. Coherent Rayleigh backscattering was identified as a significant noise source soon after fiber-based rotation sensors were first demonstrated [67]. The amplitude of this noise can be reduced by reducing the coherence length of the light source, and thereby reducing the length span over which backscattered light from one beam can combine coherently with the counter-propagating beam. However, many incoherent light sources, such as semiconductor light emitting diodes, do not possess

sufficient brightness and stability to be utilized in rotation sensing. The brightness, stability, and operating wavelength (1.5 $\mu$m) make superluminescent Er-doped fibers ideal light sources for rotation sensing [68,69].

### 3.5. Summary

Rare-earth doped ceramic materials can be tailored to provide a wide range of optical behavior, due to the ease with which ions from the entire rare-earth series can be incorporated into a large number of ceramic host materials. Through the appropriate choice of rare-earth ion, materials can be fabricated with absorption or emission bands in desired spectral locations. Further tuning of the optical behavior may be achieved via the use of multiple rare-earth dopants to independently adjust both absorption and emission characteristics. In this case, resonant energy transfer provides the required coupling between the excited state populations of the various dopant species. The choice of host material also plays an extremely important role in determining the optical behavior of the rare-earth ions. Properties such as the strengths of the optical transitions and the rate of nonradiative relaxation can be modified (within certain ranges) by appropriate choice of host material. In addition, host materials can be chosen to impart other desired properties such as chemical and environmental durability, and enhanced sensitivity to environmental factors such as temperature or pressure.

As a result of the wide latitude available for the design of rare-earth based optical materials, a large number of rare-earth doped materials have been developed for optical sensing applications, ranging in complexity from the relatively simple thermographic phosphors, to high-quality, co-doped, single mode optical fibers. In some instances, rare-earth based materials represent unique solutions to sensing problems, while in other instances sensors based upon rare-earth materials compete with other types of sensors. However, it is anticipated that technological advances will lead to more widespread use of both active and passive optical components in communications and information processing. This, in turn, will allow the inherent advantages of optical sensing technologies based on rare-earth doped ceramics to be more easily realized.

### 4. Conclusion

The ability to photo-imprint stable refractive index structures, such as Bragg gratings, into inorganic photosensitive glasses leads to a number of highly sensitive optical sensor systems. To date, the majority of the development efforts have been directed toward the use of optical fiber-based photosensitive materials. Recently, however, the development of photosensitive thin films has begun to attract considerable attention. In the case of germanosilicate glasses, photosensitivity has been linked to the presence of germanium point defects associated with oxygen vacancies. The precise nature of the mechanism dominating the refractive index change, however, is dependent upon both the materials used and the exposure conditions employed. While photosensitive materials have been successfully applied to sense, for example, strain, temperature, and vibration, continued refinement of their optical performance, as well as the development of new sensing strategies, is dependent on a fundamental understanding of the physical mechanisms responsible for photosensitivity.

Rare-earth doped optical ceramics can be tailored to suit a large number of optical sensing applications, due to the wide range of dopants and hosts available. These materials can be used as optical transducer elements (e.g. the thermographic phosphors), or can be used as light sources (e.g. superluminescent optical fibers, fiber lasers and fiber amplifiers) to probe other types of transducers. Further improvements in the optical performance of this class of materials will be achieved by developing a better understanding of the interaction between the rare-earth dopant ions and the host materials, and the subsequent development of improved dopant/host systems. An example where this strategy has already been demonstrated is the development of fluorozirconate host glasses, which drastically improve the optical efficiency of rare-earth light sources, by providing a low-phonon energy environment for the rare-earth ions, and thereby minimizing the rate of nonradiative relaxation.

### References

1. H. Poignant, S. Boj, E. Delevaque, M. Monerie, T. Taunay, P. Niay, P. Bernage, and W.X. Xie, *Elec. Lett.*, **30**, 1339 (1994).
2. M. Douay, W.X. Xie, P. Bernage, P. Niay, B. Boulard, Y. Gao, C. Jacoboni, and H. Poignant, *SPIE*, **2998**, 58 (1997).

3.  M. Asobe, T. Ohara, I. Yokohama, and T. Kaino, *Elec. Lett.*, **32**, 1611 (1996).

4.  K. Tanaka, N. Toyosawa, and H. Hisakuni, *Opt. Lett.*, **20**, 1976 (1995).

5.  K.O. Hill, Y. Fujii, D.C. Johnson, and B.S. Kawasaki, *Appl. Phys. Lett.*, **32**, 647 (1978).

6.  L. Reekie and L. Dong, *SPIE*, **2998**, 2 (1997) and references therein.

7.  M.M. Broer, R.L. Cone, and J.R. Simpson, *Opt. Lett.*, **16**, 1391 (1991).

8.  F.M. Durville, E.G. Behrens, and R.C. Powell, *Phys. Rev.*, **B34**, 4213 (1986).

9.  D.M. Krol and J.R. Simpson, *Opt. Lett.*, **16**, 1650 (1991).

10. J. Hubner, J.-M. Jouanno, J.E. Pedersen, R. Kromann, T. Feuchter, and M. Kristensen, *SPIE*, **2998**, 100 (1997).

11. J. Canning, D.J. Moss, M. Faith, P. Leach, P. Kemeny, C.V. Poulsen, and O. Leistiko, *Elec. Lett.*, **32**, 1479 (1996).

12. B.G. Potter Jr., R. Ochoa, D.G. Chen, and J.H. Simmons, *Opt. Lett.*, **17**, 1349 (1992).

13. K.D. Simmons, G.I. Stegeman, B.G. Potter Jr., and J.H. Simmons, *Opt. Lett.*, **18**, 25 (1993).

14. T. Erdogan, A. Partovi, V. Mizrahi, P.J. Lemaire, W.L. Wilson, T.A. Strasser, and A.M. Glass, *Appl. Optics*, **34**, 6738 (1995).

15. J. Nishii, H. Yamanaka, H. Hosono, and H. Kawazoe, *Opt. Lett.*, **21**, 1360 (1996).

16. K. Simmons-Potter, B.G. Potter Jr., D.C. McIntyre, and P.D. Grandon, *Appl. Phys. Lett.*, **68**, 2011 (1996).

17. B.G. Potter Jr., K. Simmons-Potter, W.L. Warren, J.A. Ruffner, and D.C. Meister, *SPIE*, **2998**, 146 (1997).

18. K.D. Simmons, S. LaRochelle, V. Mizrahi, G.I. Stegeman, and D.L. Griscom, *Opt. Lett.*, **16**, 141 (1991).

19. D.P. Hand, and P.St.J. Russell, *Opt. Lett.*, **15**, 102 (1990).

20. R.M. Atkins, V. Mizrahi, and T. Erdogan, *Elec. Lett.*, **29**, 385 (1993).

21. K.D. Simmons, G.I. Stegeman, B.G. Potter Jr., and J.H. Simmons, *J. Non-Cryst. Sol.*, **179**, 254 (1994).

22. D. Wong, S.B. Poole, and M.G. Sceats, *Opt. Lett.*, **17**, 1773 (1992).

23. J.P. Bernardin and N.M. Lawandy, *Opt. Commun.*, **79**, 194 (1990).

24. B. Poumellec, P. Guenot, I. Riant, P. Sansonetti, and P. Niay, *Opt. Mat.*, **4**, 441 (1995).

25. P. Cordier, J.C. Doukhan, E. Fertein, P. Bernage, P. Niay, J.F. Hayon, and T. Georges, *Opt. Commun.* **111**, 269 (1994).

26. J.L. Archambault, L. Reekie, and P.St.J. Russell, *Elec. Lett.*, **29**, 28 (1993).

27. P.J. Lemaire, R.M. Atkins, V. Mizrahi, and W.A. Reed, *Elec. Lett.*, **29**, 1191 (1993).

28. A. Inoue, M. Shigehara, M. Ito, M. Inai, Y. Hattori, and T. Mizunami, *Optoelec.- Dev. And Tech.*, **10**, 119 (1995).

29. R.J. Campbell and R. Kashyap, *Int. J. Optoelec.*, **9**, 33 (1994).

30. G. Meltz, W.W. Morey, and W.H. Glenn, *Opt. Lett.*, **14**, 823 (1989).

31. K.O. Hill and G. Meltz, *J. Lightwave Tech.*, **15**, 1263 (1997).

32. I. Bennion, J.A.R. Williams, L. Zhange, K. Sugden, and N.J. Doran, *Opt. and Quant. Elec.*, **28**, 93 (1996).

33. A.D. Kersey, *Opt. Fiber Tech.*, **2**, 291 (1996) and references therein.

34. S. LaRochelle, V. Mizrahi, K.D. Simmons, G.I. Stegeman, and J.E. Sipe, *Opt. Lett.*, **15**, 399 (1990).

35. A.D. Kersey, T.A. Berkoff, and W.W. Morey, *Opt. Lett.*, **18**, 72 (1993).

36. S.M. Melle, K. Liu, and R.M. Measures, *IEEE Photonics Tech. Lett.*, **4**, 516 (1992).

37. S.W. James, M.L. Dockney, and R.P. Tatam, *Elec. Lett.*, **32**, 1133 (1996).

38. S. Theriault, K.O. Hill, F. Bilodeau, D.C. Johnson, J. Albert, G. Drouin, and A. Belivean, *Opt. Rev.*, **4**, 145 (1997).

39. M.G. Xu, L. Reekie, Y.T. Chow, and J.P. Dakin, *Elec. Lett.*, **29**, 398 (1993).

40. M.A. Davis, D.G. Bellemore, and A.D. Kersey, *Cement and Concrete Comp.*, **19**, 45 (1997).

41. D.J. Moss, J. Canning, M. Faith, S. Madden, P. Kenneny, L. Poladian, F. Ladouceur, J.D. Love, C.V. Poulsen, and O. Leistiko, *SPIE*, **2998**, 142 (1997).

42. *PIRI Inc*.

43. K. Simmons-Potter et al., *Jap. J. Appl. Phys.*, in press.

44. K. Simmons-Potter, B.G. Potter Jr., D.C. Meister, and M.B. Sinclair, *J. Non-Cryst. Sol.*, submitted.

45. K. Simmons-Potter, B.G. Potter Jr., unpublished results.

46. B.G. Potter Jr., K. Simmons-Potter, and P.J. Brannon, *Elec. Lett.*, **33**, 1073 (1997).

47. J.E. Huheey, *Inorganic Chemistry*, chapter 16, (Harper and Row, New York, 1978).

48. R. Reisfeld, C.K. Jorgensen, *Lasers and Excited States of Rare Earths* (Springer-Verlag, Berlin, 1977).

49. L.A. Reisberg and M.J. Weber, in *Progress in Optics XIV*, E. Wolf, ed., p. 89 (North-Holland, Amsterdam, 1976), and references therein.

50. A.A. Kaminskii, *Crystalline Lasers: Physical Processes and Operating Schemes* (CRC Press, Boca Raton, Fl, 1996).

51. A.E. Siegman, *Lasers* (University Science Books, Mill Valley, CA, 1986).

52. M. Inokuti and F. Hirayama, *J. Chem. Phys.*, **43**, 1978 (1989).

53. T. Forster, *Ann. Physik.*, **2**, 55 (1948).

54. D.L. Dexter, *J. Chem. Phys.*, **21**, 836 (1953).

55. L.G. Van Uitert, E.F. Dearborn, and W.H. Gradkiewicz, *J. Chem. Phys.*, **49**, 4400 (1968).

56. T.F. Morse, K. Oh, and L. Reinhart, *SPIE Proceedings*, **2510**, 158 (1995).

57. The $^3H_4$ and $^3F_4$ designations used in the present work correspond to the designations used in Reference 56 and many other investigations of $Tm^{3+}$. However, there is also a large body of literature in which the designations of the $^3H_4$ and $^3F_4$ states are reversed.

58. K.T.V. Grattan and Z.Y. Zhang, *Fiber Optic Fluorescence Thermometry* (Chapman and Hall, London, 1995).

59. S.W. Allison and G.T. Gillies, *Rev. Sci. Instrum.*, **68**, 2615 (1997), and references therein.

60. K.W. Quoi, R.A. Lieberman, L.G. Cohen, D.S. Shenk, and J.R. Simpson, *IEEE Journal of Lightwave Technology*, **10**, 847 (1992).

61. G.W. Baxter, E. Maurice, and G. Monnom, *SPIE Proceedings* **2510**, 293 (1995).

62. M.C. Farries, M.E. Fermann, R.I. Laming, S.B. Polle, D.N. Payne, and A.P. Leach, *Electronics Letters*, **22**, 418 (1986).

63. E. Maurice, G. Monnom, D.B. Ostrowsky, and G. Baxter, *SPIE Proceedings*, **2360**, 219 (1994).

64. E. Maurice, G. Monnom, B. Dussardier, A. Saissy, D.B. Ostrowsky, and G.W. Baxter, *Applied Optics*, **34**, 8019 (1995).

65. B.D. MacCraith and F.J. McAleavey, *SPIE Proceedings*, **2360**, 90 (1994).

66. F.J. McAleavey and B.D. MacCraith, *Electronics Letters*, **31** 1379 (1995).

67. W.K. Burns, *Optical Fiber Rotation Sensing* (Academic Press, Boston, 1994).

68. S.K. Kim, B.Y. Kim, and H.K. Kim, *SPIE Proceedings*, **2360**, 108 (1994).

69. P.F. Wysocki, M.J.F. Digonnet, B.Y. Kim, and H.J. Shaw, *IEEE Journal of Lightwave Technology*, **12**, 550 (1994).